Angewandte Chemie
Eine Zeitschrift der Gesellschaft Deutscher Chemiker

Supporting Information

An Implantable Fiber Biosupercapacitor with High Power Density by Multi-Strand Twisting Functionalized Fibers

Z. Qian, Y. Yang, L. Wang, J. Wang, Y. Guo, Z. Liu, J. Li, H. Zhang, X. Sun, H. Peng**

SUPPORTING INFORMATION

Table of Contents

SUPPORTING INFORMATION

Experimental Procedures

Materials and chemicals. Glucose oxidase from aspergillus niger (GOx, freeze-dried powder, >180 U/mg), tetrathiafulvalene (TTF, 98%) and polyvinyl alcohol (PVA,1799) were purchased from Shanghai Aladdin Biochemical Technology Co., Ltd. Platinum on carbon (Pt/C, hispec4000) was purchased from Johnson Matthey. Nafion (5 wt% in lower aliphatic alcohols and water) was purchased from Sigma Aldrich Co., Ltd. β-D-Glucose (>85.0%) was purchased from TCI (Shanghai) Development Co., Ltd. Phosphate buffered saline (PBS, 0.1 M, pH = 7.4), paraformaldehyde fixative, hematoxylin-eosin (H&E) stain kit, 4',6-diamidino-2-phenylindole (DAPI), anti-CD68 Rabbit pAb (GB113109) and Cy3 conjugated Goat Anti-Rabbit IgG (H+L) (GB21303) were purchased from Solarbio Science and Technology Co., Ltd. All other reagents were purchased from Sinopharm Chemical Reagent Co., Ltd.

Preparation of CNT fiber. CNT fibers were fabricated by floating catalytic chemical vapor deposition. The reaction was carried out in a furnace at the temperature of 1200°C, using flowing ethanol as carbon source, thiophene and ferrocene as composite catalysts, argon (200 sccm) as carrier gas, and hydrogen (1600 sccm) as reducing gas. Continuous synthesized CNT filament bundles were then densified by water, dried and collected on the reels to form CNT fibers.

Preparation of biofuel cell electrodes. For the GOx/TTF/CNT fiber electrode, CNT fiber was first immersed in a 20 mM TTF solution for one hour with the mixed solvent of ethanol and acetone in a 9:1 volume ratio, and then washed the unstably bound TTF with deionized water. After drying at room temperature, it was immersed in a cache solution of 40 mg·mL^{-1} GOx in PBS containing 0.15% glutaraldehyde and processed overnight at 4°C to obtain the GOx/TTF/CNT fiber electrode. For the Pt/C/CNT fiber electrode, it was prepared by coating 5 mg·mL^{-1} of Pt/C catalyst dispersion on the surface of the CNT fiber electrodes and dried at room temperature. The configuration of a homogeneous Pt/C catalyst dispersion was obtained by adding 5 mg Pt/C catalyst to a mixture of deionized water, ethanol and Nafion in 75:22:3 volume ratios and ultrasonically dispersed for one hour. All electrodes were stored at 4°C until used.

Preparation of supercapacitor electrodes. A three-electrode system with CNT fiber as the working electrode, platinum wire as the counter electrode and commercial silver/silver chloride electrode as the reference electrode was used to electrochemically deposit PANI by constant voltage plating at 0.75 V in 0.1 M aniline/1 M sulfuric acid mixture solution. The plating charge was calculated based on the mass of CNT fiber to obtain a fiber supercapacitor with a 1:1 mass ratio of CNT to PANI.

Preparation of fiber BSC. The above biofuel cell electrodes, including anodes and cathodes, were integrated with the supercapacitor electrodes by fiber twisting to obtain the hybrid device. Then, the fiber electrodes were dipped in 10 wt% PVA solution and pulled out at a constant speed of 50 mm·min^{-1} controlled by a tensile machine (HY-0305, Shanghai Hengyi Precision Instrument Co., Ltd) and then repeatedly frozen three times at −20°C to obtain the PVA-coated fiber BSC. The thickness of PVA gel can be further adjusted by increasing the number of coatings or changing the dip-coating speed.

Apparatus and measurements. The structure and morphology of the fiber BSC were characterized using scanning electron microscopy (SEM, Zeiss Ultra 55). The electrochemical properties of biofuel cell, supercapacitor and fiber BSC were collected by CHI660e electrochemical workstation and Metrohm Autolab M204. Specifically, for GOx/TTF/CNT fiber, Pt/C/CNT fiber and PANI/CNT fiber, electrochemical tests were performed using a three-electrode system with the test electrode as the working electrode, platinum wire as the counter electrode, and Ag/AgCl (3M KCl) electrode as the reference electrode. The power density of the biofuel cell and the pulse performance of the fiber BSC were tested using a two-electrode system, with the cathode as the working electrode and the anode as both the counter and reference electrode. The ultrasonic photoacoustic images were obtained and analyzed *via* a Vevo LAZR Imaging System (Fuji Film VisualSonics Inc). The tension of rat leg movement was measured by a biometric signal acquisition and analysis system (MD3000) and muscle tension transducer (ZH-HU-1).

Relevant calculations. All calculations of electrochemical properties were based on geometric surface areas of fiber electrodes.
The equivalent series resistance in Ω, can be calculated according to Ohm's law:

$$ESR = \Delta V_{ohmic} / i_{pulse} \quad \text{(S1)}$$

where i_{pulse} is the applied current in A and ΔV_{ohmic} is the ohmic drop in V.
The power density for each pulse discharge, P, in mW·cm^{-2} was determined by the following equation[1]:

$$\begin{aligned} P &= i_{pulse} \times V_{pulse} = i_{pulse} \times \left(V_{cutoff} - \Delta V_{ohmic} - \Delta V_{discharge}\right) \\ &= i_{pulse} \times \left(V_{cutoff} - ESR \times i_{pulse} - i_{pulse} \times t_{pulse}/C_p\right) \end{aligned} \quad \text{(S2)}$$

where V_{pulse} is the instant potential at the end of each discharge; V_{cutoff} is the maximal potential the hybrid device can reach for each reset; $\Delta V_{discharge}$ is the voltage drop during each pulse discharge; t_{pulse} is the constant time of each pulse; C_p is the capacitance of BSC.

In vivo experiments. Experimental rats (SD, male, 6–8 weeks) were purchased from Shanghai Slaughter Laboratory Animal Co. All animal experiments were conducted in accordance with the protocol approved by the Animal Experimentation Committee of Fudan University with the approval number of SYXK2020-0032. All animals were handled in strict compliance with the operational requirements of the National Institutes of Health and Fudan University. After all preoperative cleanings, the rats were anaesthetized with 2% isoflurane and placed smoothly on a surgical positioning table. The fiber BSC was implanted into the subcutaneous tissue of rats with the aid of a syringe and fixed by bio-glue (3M). After connecting the circuit, the power output performance of the fiber BSC

was recorded *in vivo*. Stimulation of the sciatic nerve was performed by connecting CNT fiber extensions. The rat leg was connected to the MD3000 pulley accessory *via* a thin flexible wire to record undirected leg movements. All *in vivo* tests were repeated on three different rats.

Hematoxylin-eosin (H&E) staining and Immunohistochemistry test. One week after the implantation of fiber BSC, rat skin tissue containing the implanted device was cut out and put in paraformaldehyde fixative. The tissue was dehydrated using a gradient concentration of ethanol and then embedded in paraffin wax. The paraffin blocks were sliced into 6 μm thick sections and stored at room temperature. For H&E staining, slices were processed with xylene, anhydrous ethanol, 75% ethanol and water. Hematoxylin staining was completed by immersing slices for 3–5 minutes in differentiation solution, reblue solution, and hematoxylin staining solutions in that order. After that, we re-dehydrated the slices and finished their eosin staining by dipping them in the staining solution for 5 minutes. A water rinse was performed on the samples before each solution change. Prior to immunostaining, slices were antigenically repaired using citrate buffer and then incubated for 30 min with BSA solution. Anti-CD68 Rabbit pAb (1:200) was used as the primary antibody. Cy3 conjugated Goat Anti-Rabbit lgG (H+L) (1:300) was used as the secondary antibody. DAPI was used to stain the nucleus of all cells. Each group comprised three rats. The slices were observed under fluorescence microscopy (Olympus BX51).

Results and Discussions

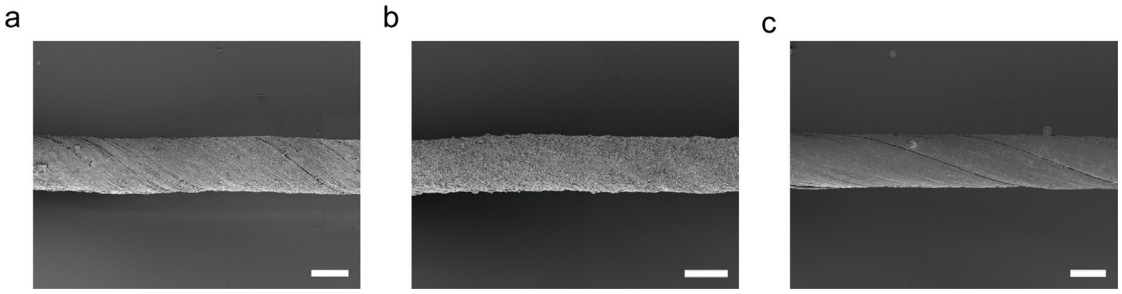

Figure S1. SEM images of a) GOx/TTF/CNT fiber, b) Pt/C/CNT fiber and c) PANI/CNT fiber. Scale bar, 50 µm.

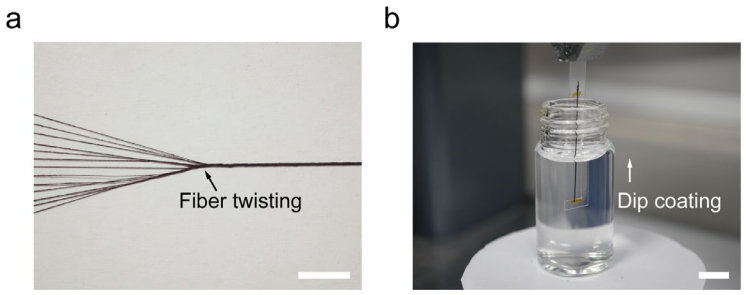

Figure S2. Photographs of preparation process of fiber BSC. a) Fiber twisting process. Scale bar, 0.5 cm. b) PVA dip-coating process. Scale bar, 1 cm.

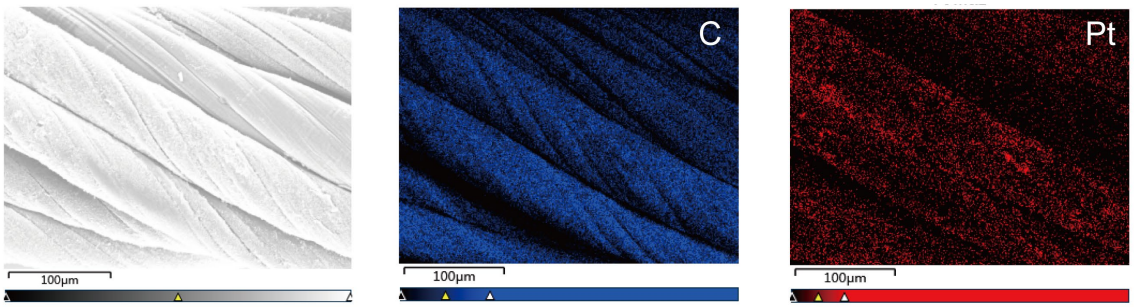

Figure S3. The distinguishable modification of different functional layers on CNT fibers showed by the elemental (C, Pt) mapping images of fiber BSC cathode. Significant elemental differences were observed between Pt/C/CNT fibers and PANI/CNT fiber without platinum element.

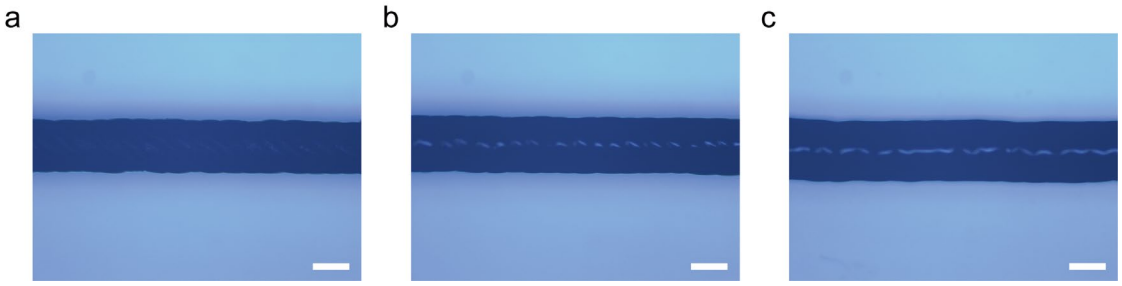

Figure S4. Optical micrographs of fiber BSC electrodes a) before PVA coating, b) coated with PVA once and c) coated with PVA for three times. The thicknesses of PVA layer were about 6 and 20 μm in (b) and (c), respectively. Scale bar, 200 μm.

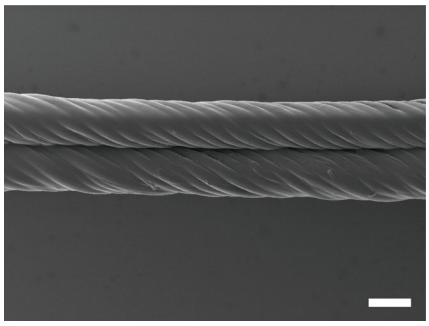

Figure S5. SEM image of a fiber BSC with two electrodes placed in parallel. Scale bar, 300 μm.

The distance between the two fiber BSC electrodes was 23.0 ± 3.5 μm.

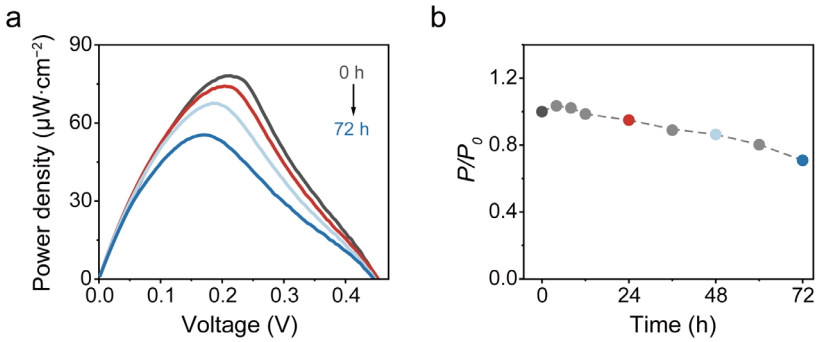

Figure S6. Long-term stability of the fiber biofuel cell. a) The power density–voltage curves of fiber biofuel cell in 4 mM glucose solution at different periods. The sweep rate was 5 $mV \cdot s^{-1}$. b) The calculated relative change of maximal power density of fiber biofuel cell after three days.

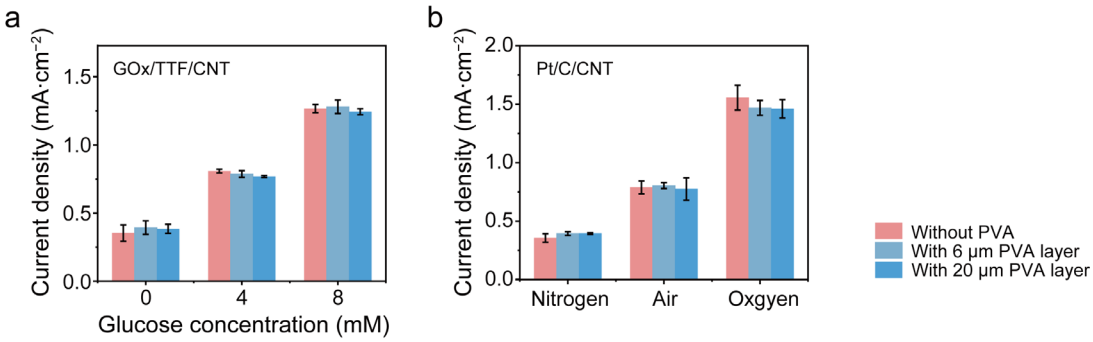

Figure S7. Comparison of the electrochemical performance of fiber electrodes without PVA and with PVA layer at thickness of 6 and 20 μm. a) The current density (at 0 V) of GOx/TTF/CNT fibers in 0, 4 and 8 mM glucose solution (n = 3). b) The current density (at 0.2 V) of Pt/C/CNT fibers in nitrogen-saturated, air-saturated and oxygen-saturated PBS (n = 3).

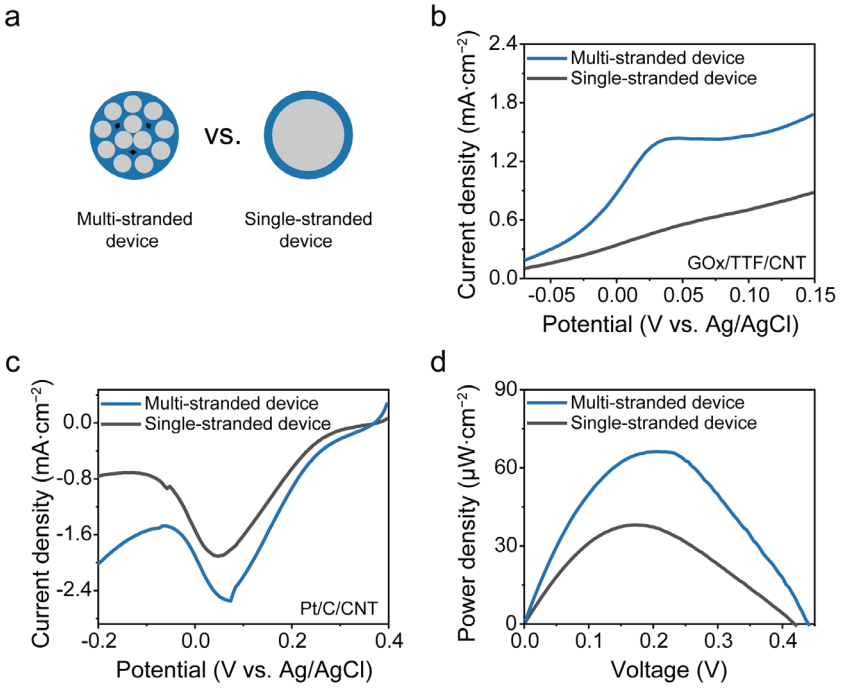

Figure S8. Comparison of the single-stranded device and twisted multi-stranded device. a) Schematic diagram of the single-stranded device and twisted multi-stranded device. b) Linear sweep voltammograms of GOx/TTF/CNT fibers in a 4 mM glucose solution at 5 $mV \cdot s^{-1}$. c) Linear sweep voltammograms of Pt/C/CNT fibers in air-saturated PBS at 5 $mV \cdot s^{-1}$. d) The power density–voltage curves of biofuel cells in a 4 mM glucose solution.

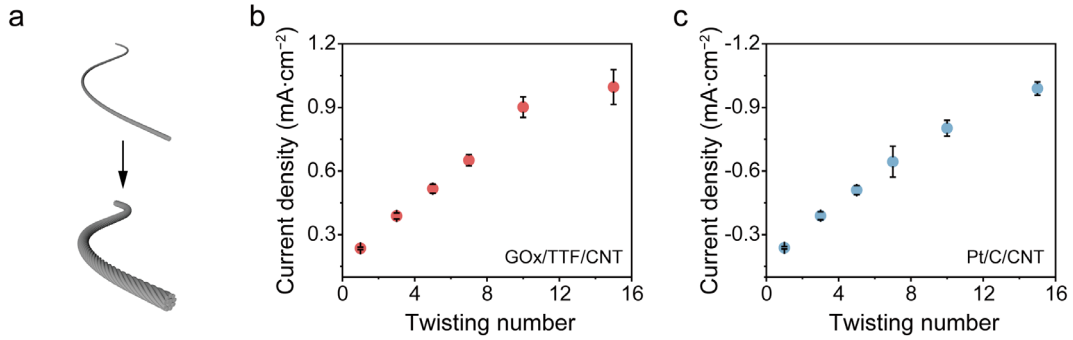

Figure S9. Evolution of fiber biofuel cells with different twisting fiber numbers. a) Schematic diagram of multiple fiber twisting. b) The anodic current density (at 0 V) of GOx/TTF/CNT fibers with different twisting fiber numbers (n = 3). c) The cathodic current density (at 0.2 V) of Pt/C/CNT fibers with different twisting fiber numbers (n = 3).

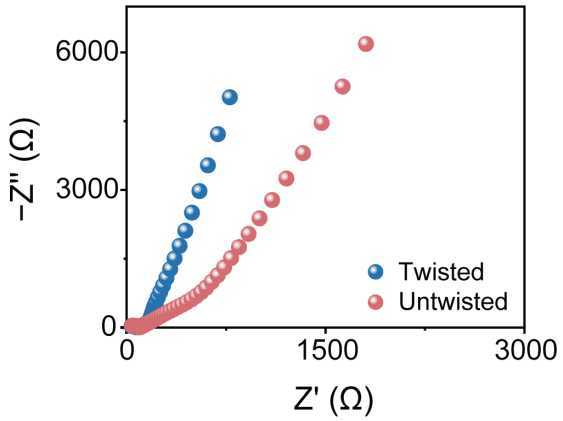

Figure S10. Nyquist plots of the twisted and untwisted CNT fiber electrodes at 0 V from 100 kHz to 0.01 Hz in PBS.

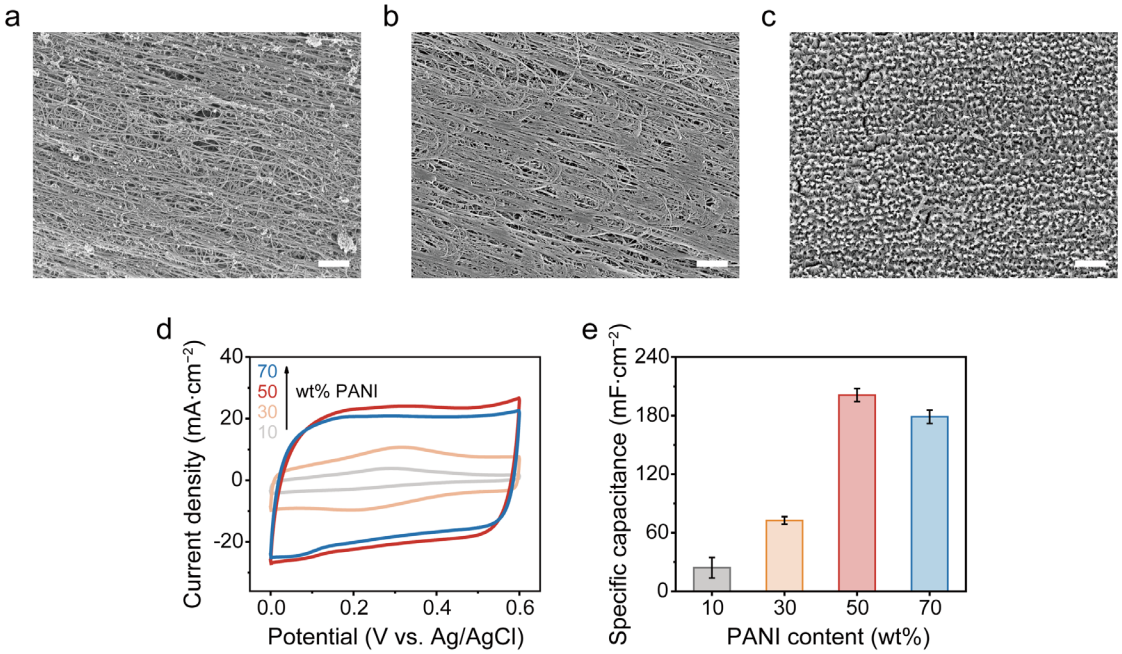

Figure S11. Comparison of PANI/CNT fibers with 10–70 wt% PANI. a–c) SEM images of CNT fibers with 10 wt% (a), 30 wt% (b), 70 wt% (c) PANI. Scale bar, 1 µm. d) Cyclic voltammograms of CNT fibers with 10–70 wt% PANI at sweep rates of 100 $mV \cdot s^{-1}$. e) The resulting calculated capacitance values (n = 3).

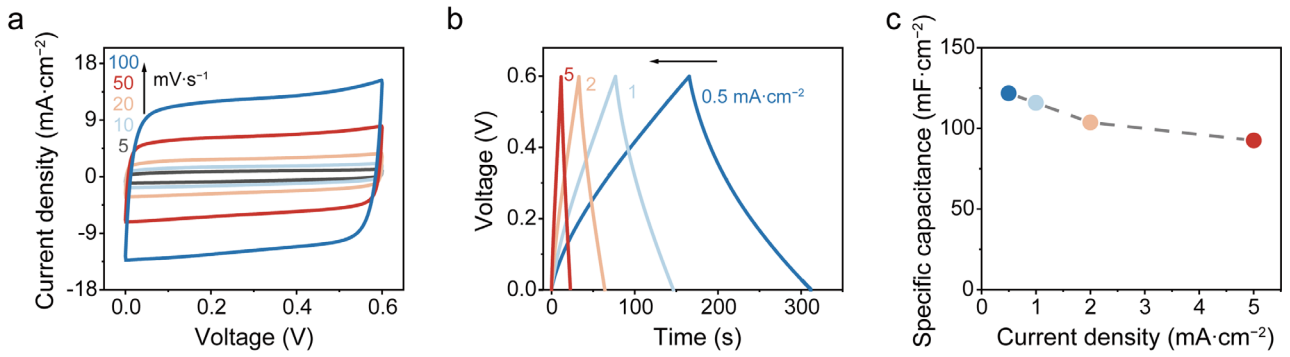

Figure S12. Electrochemical performances of PANI/CNT supercapacitor. a) Cyclic voltammograms of PANI/CNT fiber at sweep rates of 5–100 mV·s^{-1}. b) Galvanostatic charge–discharge curves of PANI/CNT fiber with current densities of 0.5–5 mA·cm^{-2}. c) The calculated specific capacitance at 0.5–5 mA·cm^{-2} current densities from galvanostatic charge–discharge curves.

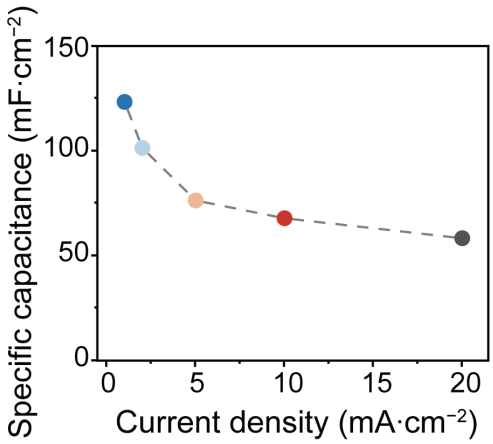

Figure S13. The specific capacitance of fiber BSC at 1–20 mA·cm^{-2} current densities calculated from galvanostatic charge–discharge curves.

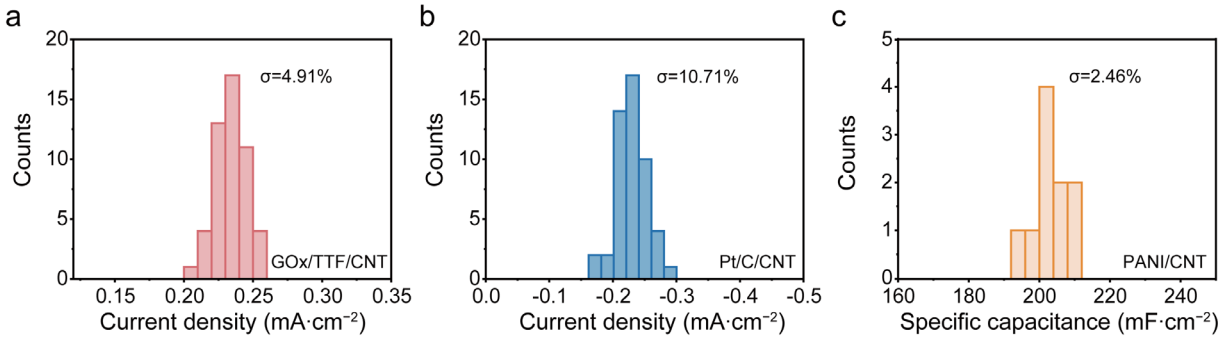

Figure S14. Performance consistency of fiber electrodes. a, b) Distribution of the catalytic current densities of 50 GOx/TTF/CNT fiber electrodes (at 0 V) and 50 Pt/C/CNT fiber electrodes (at 0.2 V). c) Distribution of the specific capacitances of 10 PANI/CNT fiber electrodes.

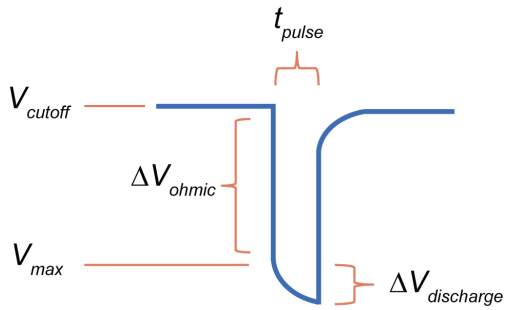

Figure S15. Illustration for the pulse discharge of the fiber BSC. ΔV_{ohmic} indicates the ohmic drop upon the application of current pulse; V_{cutoff} indicates the maximal potential the hybrid device can reach for each reset; V_{max} indicates the voltage at the beginning of capacitive discharge; $\Delta V_{discharge}$ indicates the voltage drop during each pulse discharge; t_{pulse} indicates the constant time of each pulse.

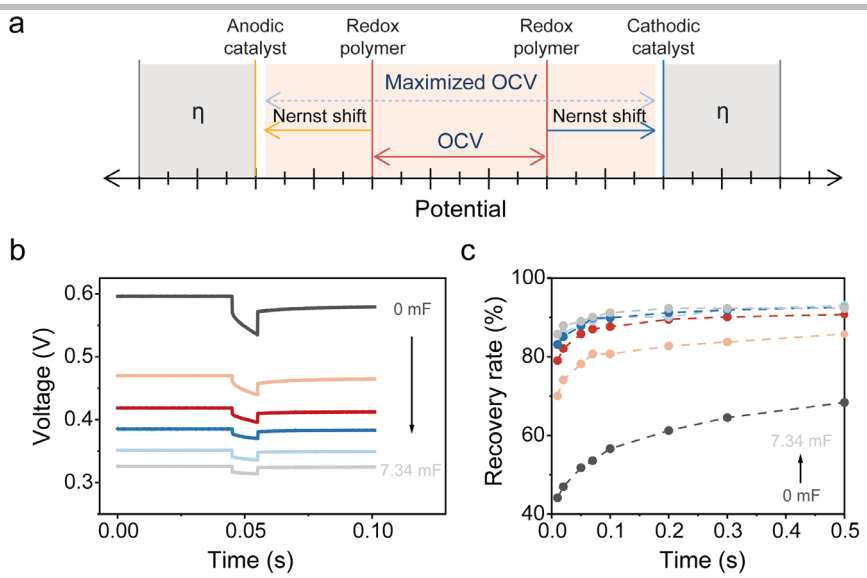

Figure S16. Optimization of the composition of supercapacitors in fiber BSC. a) Schematic illustration of the redox potential involved in fiber BSC. Anodic catalyst indicates the redox potential of GOx. Cathodic catalyst indicates the redox potential of Pt/C. Redox polymer indicates the redox potential of PANI at different redox states. η indicates the overpotential required for the catalyst to convert the fuel. OCV indicates the open-circuit voltage of fiber BSC. b) Pulse discharge curves of fiber BSC with capacitance from 0 to 7.34 mF at current value of 0.5 mA. c) Recording of the recovery of the OCV after pulse discharge at 0.5 mA.

In BSCs, the redox potential shift of the pseudocapacitive material depending on its characteristics and content, would affect the maximal open-circuit voltage and thus the effective power output.

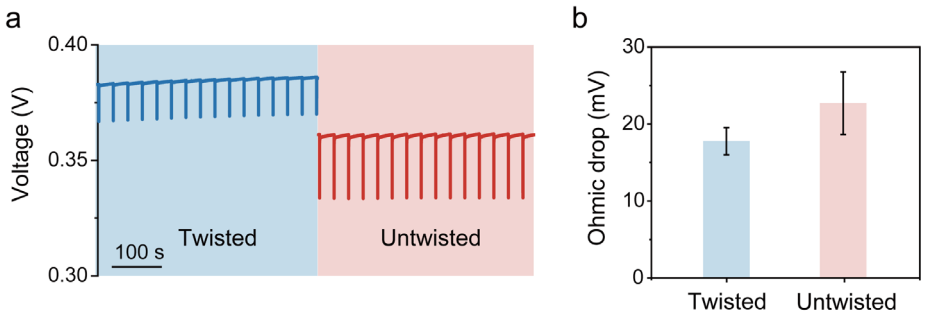

Figure S17. Comparison of pulse discharge performance of the twisted and untwisted fiber BSCs. a) Pulse discharge curve. b) The ohmic drop (n = 3).

The twisted device showed a higher initial voltage while a lower ohmic voltage drop than the untwisted one, indicating a lower internal resistance.

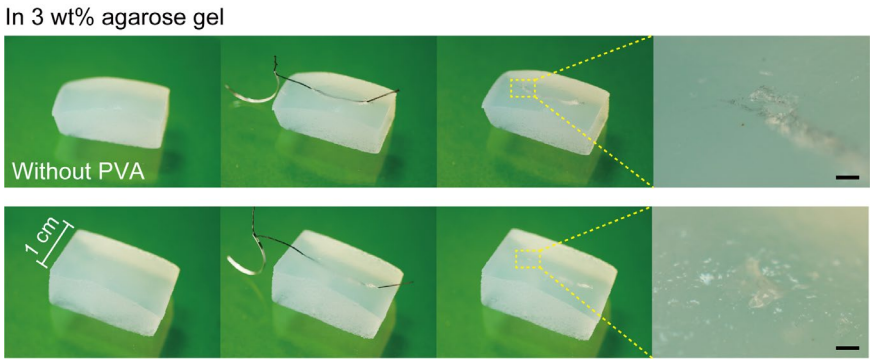

Figure S18. Photographs of fiber BSCs with and without PVA coating across the 3 wt% agarose gel. Scale bar, 200 μm.

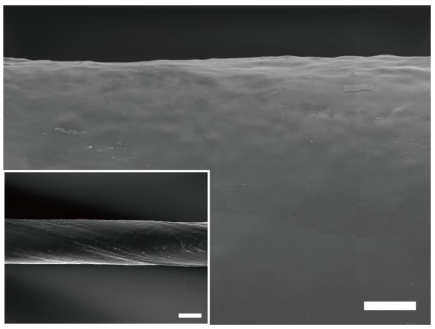

Figure S19. SEM images of fiber BSC after friction of 3 wt% agarose gel. Scale bar, 20 μm, (inset) 100 μm.

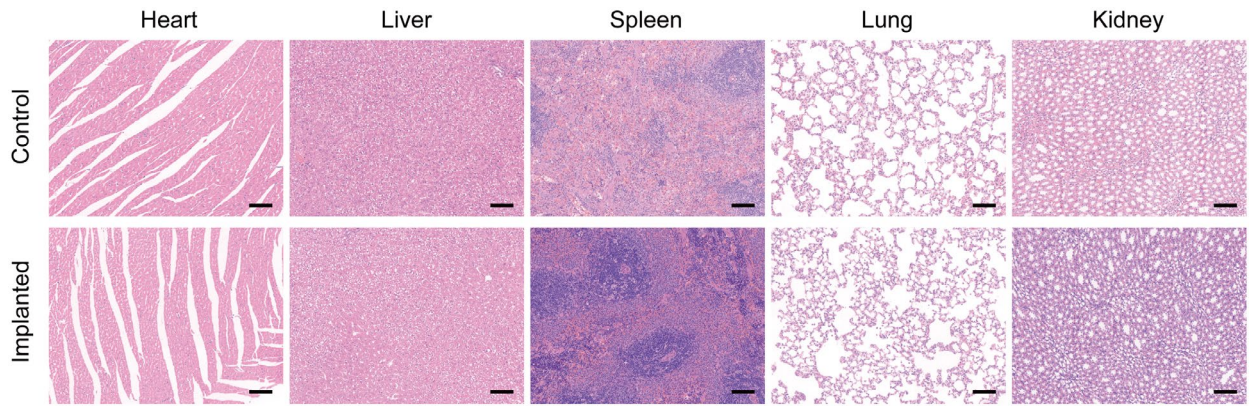

Figure S20. H&E staining of the major organs of rats with and without implanted fiber BSCs for one week. Scale bar, 100 μm.

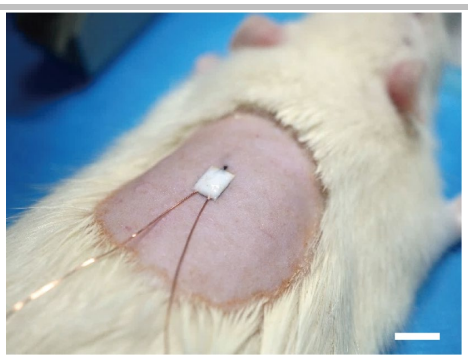

Figure S21. Photograph of the fiber BSC implanted in the subcutaneous tissue of a live rat. Scale bar, 1 cm.

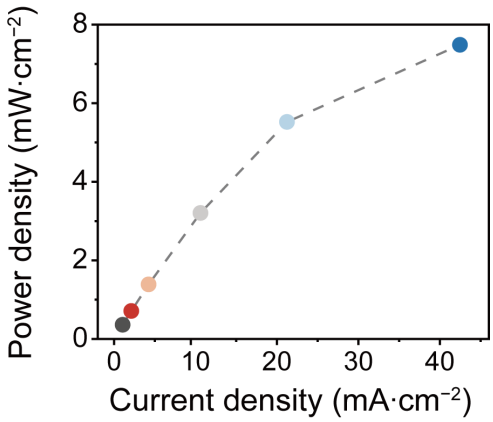

Figure S22. Calculated pulse power density of the implanted fiber BSC *in vivo* at increasing discharge current densities.

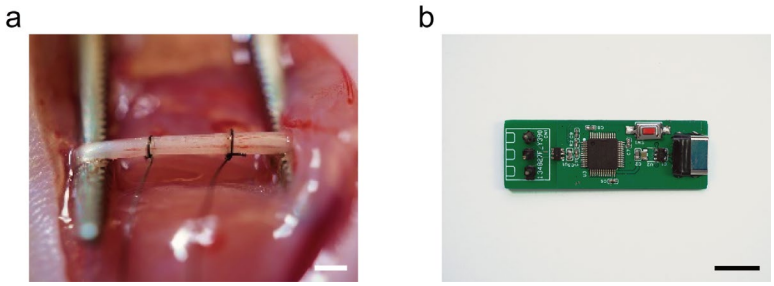

Figure S23. Photographs of the sciatic nerve stimulation and control system. a) Photograph of stimulation using CNT fiber to connect the sciatic nerve. Scale bar, 20 mm. b) Photograph of the control system. Scale bar, 1 cm.

SUPPORTING INFORMATION

Table S1. Comparison of pseudocapacitive materials used in biosupercapacitors and their operation conditions.

Material of supercapacitor	Measurement	Specific capacitance	Discharging current density/Scan rate	Discharging/scanning voltage range	Ref.
$Os(bpy)_2PVI$	GCD	391.9 ± 2.1 $\mu F \cdot cm^{-2}$	10 $\mu A \cdot cm^{-2}$	0–0.5 V	[1]
PANI	GCD	600 $mF \cdot cm^{-2}$	50 $mA \cdot g^{-1}$	0–0.3 V	[2]
PPy	GCD	27.2 $mF \cdot cm^{-2}$	0.1 $mA \cdot cm^{-2}$	0–0.6 V	[3]
PANI	CV	1.6 ± 0.2 $mF \cdot cm^{-2}$	10–500 $mV \cdot s^{-1}$	-	[4]
PANI	**GCD**	**123 $mF \cdot cm^{-2}$**	**1 $mA \cdot cm^{-2}$**	**0–0.6 V**	**This work**

Os(bpy)2PVI: $[Os(2,2'\text{-bipyridine})_2(polyvinylimidazole)_{10}Cl]^{+/2+}$; PPy: polypyrrole; GCD: galvanostatic charge–discharge; CV: cyclic voltammogram.

SUPPORTING INFORMATION

Table S2. The recording capacitance of 10 biofuel cell fibers combined with 0–5 PANI/CNT fibers.

	Glucose/oxygen biofuel cell	+ 1 PANI/CNT fiber	+ 2 PANI/CNT fibers	+ 3 PANI/CNT fibers	+ 4 PANI/CNT fibers	+ 5 PANI/CNT fibers
Capacitance (mF)	0.68	2.34	3.16	4.18	4.82	7.34

Table S3. Comparison of power density, current density and operational lifetime of our work with previously reported BSCs.

Combination of biofuel catalysts	Material of supercapacitor	Biofuel	P_{max} ($mW \cdot cm^{-2}$)	I_{max} ($mA \cdot cm^{-2}$)	Lifetime	Ref.
FAD-GDH/BOx	$Os(bpy)_2PVI$	20 mM glucose	0.609	2	1300 pulses	[1]
CDH/BOx	PANI	50 mM glucose	1.2	3.1	25 h	[2]
LOx/Pt	PPy	10 mM lactate	1.7	10	12 h, 1440 pulses	[3]
FDH/Lac	PANI	25 mM fructose	4.8	11.7	8 h	[4]
GOx/Lac	CNT	200 mM glucose	12.3	34.6	40000 pulses	[5]
GDH/BOx	Buckypaper	100 mM glucose	0.87	4	4200 cycles	[6]
GDH/BOx	ITO NPs	50 μM glucose	0.03	0.02	17 h, 100 cycles	[7]
GOx	ITO/rGO	11 mM glucose	0.62	3.05	-	[8]
GOx/Pt/C	**PANI**	**4 mM glucose**	**22.6**	**106.2**	**72 h, 8640 pulses**	**This work**

FAD-GDH: flavin adenine dinucleotide-dependent glucose dehydrogenase; BOx: bilirubin oxidase; Os(bpy)2PVI: $[Os(2,2'\text{-bipyridine})_2(polyvinylimidazole)_{10}Cl]^{+/2+}$; CDH: cellobiose dehydrogenase; Lac: laccase; GDH: glucose dehydrogenase; ITO NPs: indium tin oxide nanoparticles; LOx: lactate oxidase; PPy: polypyrrole; FDH: fructose dehydrogenase; rGO: reduced graphene oxide.

References

[1] X. Xiao, P. O. Conghaile, D. Leech, R. Ludwig, E. Magner, *Biosens. Bioelectron.* **2017**, *90*, 96–102.
[2] D. Pankratov, Z. Blum, D. B. Suyatin, V. O. Popov, S. Shleev, *Chemelectrochem* **2014**, *1*, 343–346.
[3] J. Lv, L. Yin, X. Chen, I. Jeerapan, C. A. Silva, Y. Li, M. Le, Z. Lin, L. Wang, A. Trifonov, S. Xu, S. Cosnier, J. Wang, *Adv. Funct. Mater.* **2021**, *31*, 2102915.
[4] P. Bollella, Z. Boeva, R.-M. Latonen, K. Kano, L. Gorton, J. Bobacka, *Biosens. Bioelectron.* **2021**, *176*, 112909.
[5] C. Agnes, M. Holzinger, A. Le Goff, B. Reuillard, K. Elouarzaki, S. Tingry, S. Cosnier, *Energ. Environ. Sci.* **2014**, *7*, 1884–1888.
[6] C. W. N. Villarrubia, F. Soavi, C. Santoro, C. Arbizzani, A. Serov, S. Rojas-Carbonell, G. Gupta, P. Atanassov, *Biosens. Bioelectron.* **2016**, *86*, 459–465.
[7] T. Bobrowski, E. G. Arribas, R. Ludwig, M. D. Toscano, S. Shleev, W. Schuhmann, *Biosens. Bioelectron.* **2018**, *101*, 84–89.
[8] H.-J. Kil, S.-R. Kim, J.-W. Park, *Acs. Appl. Mater. Inter.* **2022**, *14*, 3838–3848.

Author Contributions

Z. Q. conceived and designed the experiments. X. S. and H. P. directed the project. Z. Q., Y. Y. and H. Z. fabricated and characterized the devices. Z. L. and J. L. implemented the stimulation control system. Z. Q. and Y. Y. conducted animal experiments. Z. Q., L. W., J. W. and Y. G. analyzed the data. All authors reviewed and critiqued the results, and made key revisions to the manuscript.